Measuring parameters of massive black hole binaries with partially aligned spins

Citation: Lang, Ryan, Scott Hughes, and Neil Cornish. "Measuring parameters of massive black hole binaries with partially aligned spins." Physical Review D 84 (2011): n. pag. Web. 8 Nov. 2011.

As Published: http://dx.doi.org/10.1103/PhysRevD.84.022002

Publisher: American Physical Society

Persistent URL: http://hdl.handle.net/1721.1/66968

Version: Final published version: final published article, as it appeared in a journal, conference proceedings, or other formally published context

PHYSICAL REVIEW D **84,** 022002 (2011)

Measuring parameters of massive black hole binaries with partially aligned spins

Ryan N. Lang,[1] Scott A. Hughes,[2] and Neil J. Cornish[3]

[1]*Gravitational Astrophysics Laboratory, NASA Goddard Space Flight Center, 8800 Greenbelt Road, Greenbelt, Maryland 20771, USA*
[2]*Department of Physics and MIT Kavli Institute, MIT, 77 Massachusetts Avenue, Cambridge, Massachusetts 02139, USA*
[3]*Department of Physics, Montana State University, Bozeman, Montana 59717, USA*

(Received 18 January 2011; published 12 July 2011)

The future space-based gravitational wave detector LISA will be able to measure parameters of coalescing massive black hole binaries, often to extremely high accuracy. Previous work has demonstrated that the black hole spins can have a strong impact on the accuracy of parameter measurement. Relativistic spin-induced precession modulates the waveform in a manner which can break degeneracies between parameters, in principle significantly improving how well they are measured. Recent studies have indicated, however, that spin precession may be weak for an important subset of astrophysical binary black holes: those in which the spins are aligned due to interactions with gas. In this paper, we examine how well a binary's parameters can be measured when its spins are partially aligned and compare results using waveforms that include higher post-Newtonian harmonics to those that are truncated at leading quadrupole order. We find that the weakened precession can substantially degrade parameter estimation. This degradation is particularly devastating for the extrinsic parameters sky position and distance. Absent higher harmonics, LISA typically localizes the sky position of a nearly aligned binary a factor of $\sim$6 less accurately than for one in which the spin orientations are random. Our knowledge of a source's sky position will thus be worst for the gas-rich systems which are most likely to produce electromagnetic counterparts. Fortunately, higher harmonics of the waveform can make up for this degradation. By including harmonics beyond the quadrupole in our waveform model, we find that the accuracy with which most of the binary's parameters are measured can be substantially improved. In some cases, parameters can be measured as well in partially aligned binaries as they can be when the binary spins are random.

DOI: 10.1103/PhysRevD.84.022002 PACS numbers: 04.80.Nn, 04.30.Db, 04.30.Tv

I. INTRODUCTION

The coalescence of massive black hole binaries is a primary source for the future space-based gravitational wave (GW) detector LISA.[1] LISA will be able to detect such sources with extremely high signal-to-noise ratio (SNR) $\gtrsim 1000$ at low redshift ($z \sim 1$), as well as with moderate, but still reasonable, SNR $\sim$10 at extremely high redshift ($z \sim 20$) [1]. Estimated event rates for these sources vary widely based on formation scenarios but tend to predict roughly tens of sources per year, with $\sim$1 as a pessimistic estimate and $\sim$100 as an optimistic one [2]. (The actual detection rate will, of course, tell us much about the formation of black hole binaries and the growth of massive black holes in the universe.)

While the detection of gravitational waves from these sources will certainly be interesting for its own sake, attention has turned in recent years to the capabilities of LISA as a true astronomical observatory. Many papers [3–7,9–20] have investigated just how well LISA can measure the parameters of the binaries it detects. This is often done using the Fisher-matrix method [20,21], which essentially measures the local curvature of the posterior probability distribution for parameters in the vicinity of the maximum. Parameters for which the posterior is more strongly curved (i.e., which more strongly affect the waveform) are measured more accurately than those for which the posterior is only weakly curved. Correlations between parameters are also extremely important. When two parameters are strongly correlated, it is difficult to ''detangle'' the influence of one on the waveform over the other. This means that the accuracy with which both parameters are measured is controlled by the one which is most poorly determined.

Recent studies have considered how well parameters can be measured while doing the actual data analysis problem of removing signals from noise [22]. In effect, these studies simulate the parameter extraction process with enough detail to uncover issues such as multiple extrema of the posterior surfaces which are missed by the simpler (and cruder) Fisher analyses. Such ''realistic'' studies are typically much more CPU-intensive and cannot easily study parameter measurement issues over a broad swath of astrophysically important parameter space. Both families of studies have substantially advanced our understanding of LISA's science reach in the past 5 or so years.

Some parameters that are especially interesting are the *intrinsic* system properties, namely, the masses and spins of the black holes. Masses can be measured extremely well in the best cases [with a relative error of $\sim 10^{-3}$ for individual masses and $\sim 10^{-5}$ for the chirp mass $\mathcal{M} \equiv m_1^{3/5} m_2^{3/5}/(m_1 + m_2)^{1/5}$]. Spins are not measured quite

[1]http://lisa.nasa.gov

so well but are still expected to be determined with percent-level accuracy. By measuring these parameters for many systems, one can construct a merger history of black holes, and by extension, their host galaxies, learning much about galaxy formation, black hole formation, AGN feedback, and so forth.

We are also interested in measuring parameters *extrinsic* to the system, namely, its position on the sky and its luminosity distance. With the position and distance (converted into an approximate redshift), astronomers can search the sky for probable electromagnetic counterparts to the gravitational wave events. Various types of counterparts have been proposed, from signals during the inspiral [23], to bright flashes at the time of merger [24] (or even reductions in luminosity [25]), to long-delayed afterglows [26]. The different scenarios arise because the behavior of gas around an inspiraling binary system is not well understood. A very different kind of electromagnetic counterpart can be produced by a kicked remnant black hole that triggers a telltale sequence of stellar disruptions [27]. (Tidal disruption of stars may also allow us to flag the presence of a binary long before it enters the LISA band, allowing a better understanding of the space density of massive black hole binaries [28].) If a counterpart can be identified, the electromagnetic information can be combined with the gravitational information to reveal more about the astrophysics of the system. Counterparts may also make it possible for binary black holes to be used as probes of the cosmological distance-redshift relation, since the electromagnetic redshift and gravitational distance are determined independently [7]. Unfortunately, finding a counterpart, even if a unique signature does exist, will not be easy. The typical error windows for LISA are $\sim$ tens of arcminutes on a side at the end of inspiral, reduced from several square degrees in the weeks and months before merger. Still, this localization does give large survey telescopes like LSST (field of view $\sim$10 square degrees) a chance to study a particular area of the sky with advance warning [29].

One particularly important result in the study of LISA's science capabilities was the discovery that including spin precession effects in the waveform model typically improves the accuracy of parameter measurement [5,9]. Spin precession arises because of geodetic and gravitomagnetic general relativistic effects [30,31]. The orbital plane of the system also precesses in order to preserve the total angular momentum on time scales shorter than the radiation reaction time. Together, these precessions modulate the amplitude and phase of the waveform, breaking correlations between certain sets of parameters and improving how well the members of those sets can be measured. The greatest improvement is to the measured masses of a binary's members (accuracy typically improved by 1–2 orders of magnitude). The measured sky position angles and distance to the source are all improved by about half an order of magnitude, reducing the size of the sky position pixel in which one must search for a counterpart by a factor of $\sim$10 (or the 3D voxel volume by a factor of $\sim$30).

The precession of one of the spins in a binary, to 1.5 post-Newtonian order and averaged over an orbit,[2] is given by

$$\dot{\mathbf{S}}_1 = \frac{1}{r^3}\left[\left(2+\frac{3}{2}\frac{m_2}{m_1}\right)\mu\sqrt{Mr}\hat{\mathbf{L}}\right]\times\mathbf{S}_1 + \frac{1}{r^3}\left[\frac{1}{2}\mathbf{S}_2 - \frac{3}{2}(\mathbf{S}_2\cdot\hat{\mathbf{L}})\hat{\mathbf{L}}\right]\times\mathbf{S}_1, \tag{1.1}$$

where $\mathbf{S}_1$ and $\mathbf{S}_2$ are the two spins, m_1 and m_2 are the two masses, $M = m_1 + m_2$ is the total mass, $\mu = m_1 m_2/M$ is the reduced mass, $\hat{\mathbf{L}}$ is the direction of the orbital angular momentum, and r is the orbital separation in harmonic coordinates. It is clear that precession is maximal when the spins of the system are orthogonal to the orbital angular momentum and to each other and vanishes when the spins and orbital axis are aligned. In [9] (hereafter Paper I), it was assumed that the relative orientation of the spins and the orbital angular momentum was completely arbitrary. The results of that paper are summarized in a series of histograms describing parameter measurement accuracy when the various angular momentum vectors are allowed to point in any direction.

Recent studies have shown, however, that accreting gas in a system may evolve the spin in such a way that the spins are at least partially aligned with each other and with the orbit [32,33]. The degree of alignment depends on the temperature of the gas: In "hot gas" models, which have polytropic index $\gamma = 5/3$, the spins align within 30° of the orbital axis. "Cold gas" models with $\gamma = 7/5$ align even more thoroughly, to within 10° [33].

Does spin-induced precession, now constrained by initial conditions, still break degeneracies as efficiently as described in Paper I? Any degradation in parameter measurement capability could have a strong effect on the ability to find electromagnetic counterparts. The results of [9,13,15] may be biased toward gas-free "dry" mergers, severely underestimating localization errors in gaseous "wet" mergers—the very systems which we are most likely to see electromagnetically. The effect of alignment on mass and spin measurements is also interesting (though

[2]The validity of averaging over an orbit can be quickly checked by comparing the precession time scale $T_{\rm prec}$ with the orbital time scale $T_{\rm orb}$. For an equal-mass system, these time scales are roughly equivalent when $r \sim 7M/8$, where M is total mass. The orbit-averaged approximation is therefore quite good for most of the inspiral waveform but will begin to break down as we approach $r \sim (2\text{–}3)M$. At these radii, the post-Newtonian approximation breaks down as well, so our use of the precession equations there is best considered to be qualitatively indicative of the relevant physics, if not numerically exact.

arguably less so, since even a factor of several degradation for these parameters would still imply excellent accuracy).

The goal of this paper is to answer the question posed above. We do so with a Fisher-matrix analysis of parameter measurement for binaries whose spins are partially aligned according to two wet merger models: hot gas, which aligns the spins and orbit to within 30°, and cold gas, which aligns to within 10°. We demonstrate that this degree of alignment can substantially degrade parameter accuracy but that one can ''repair'' much of this degradation by using the ''full'' waveform model, including harmonics beyond the leading quadrupole. In what follows, we will use the terms ''gas-free'' or ''dry'' interchangeably with the term ''random spins,'' ''hot gas'' interchangeably with the phrase ''spins aligned within 30°,'' and ''cold gas'' interchangeably with the phrase ''spins aligned within 10°.'' We also sometimes write ''30° alignment'' as shorthand for ''spins aligned within 30°,'' and likewise for ''10° alignment.'' (The two distributions contain systems with alignments less than 30° or 10°, although with a bias toward the upper end of the allowed range.)

The outline of the paper is as follows. We begin in Sec. II by describing the operation of our code, including the production of binary black hole waveforms, the LISA response, the noise model, and how we construct the Fisher matrix. We focus on changes from Paper I, leaving detailed description of the theory to that paper.

In Sec. III, we then present results for parameter errors in wet mergers, examining both ''hot'' and ''cold'' models. We compare these results to the case of dry mergers, in which spin orientations are chosen to be completely random with respect to each other and to the orbital angular momentum. It should be emphasized that throughout Sec. III, we consider only the leading quadrupole piece of the gravitational waveform (the so-called ''restricted'' post-Newtonian approximation). As expected, we find that spin alignment largely degrades LISA's ability to measure parameters. As a rough rule of thumb, we find that extrinsic parameters (sky position angles and luminosity distance) are measured a factor of $\sim$1.5–2 less accurately for 30° alignment and a factor of $\sim$2–3 less accurately for 10° alignment. In the second case, alignment eliminates most of the advantage gained by adding precession in Paper I. We find that the impact upon measured masses and spins depends strongly on mass ratio, with degradation by a factor $\sim$1–3 at 30° alignment, and a factor $\sim$1–9 at 10° alignment. We find a handful of cases in which partially aligned binaries actually do *better* than the randomly oriented systems. As we describe in Sec. III, this is due to alignment increasing these systems' average SNR.

To combat this degradation, we introduce another degeneracy-breaking effect. Much early work in LISA parameter estimation made use of the restricted waveform model, in which only the quadrupole harmonic of the orbital phase was included and only the leading ''Newtonian'' amplitude term was used with this harmonic (although the phase was constructed to high post-Newtonian order). This was done because the quadrupole harmonic dominates signal power, while the phase is the primary source of information about the signal. However, it has since been shown by several groups that including higher harmonics (and their post-Newtonian amplitudes, making the so-called full waveform model) also breaks degeneracies and reduces parameter errors [10–12,14]. The magnitude of the effect is comparable to the improvement seen by including spin precession. Recently, Klein *et al.* have presented an analysis combining both spin precession and higher harmonics [16]. A similar analysis, based on an earlier version of our own code, was conducted by the LISA Science Team to investigate the science reach of the LISA mission; the results of this study are summarized in Ref. [34].

In Sec. IV, we replace the leading quadrupole waveform with the full waveform. For the case of random spins, our answers can be compared (with some caveats) to the results of [16]. We also compute the errors for wet, partially aligned binaries with the full waveform. When higher harmonics are included, parameter errors for partially aligned binaries are often no worse, or even better, than for the case of random spins and no higher harmonics. In these particular cases, higher harmonics can more than make up for the degraded impact of spin precession. We find this degree of improvement for the minor axis of the sky position error ellipse and for the luminosity distance in a majority of (mass) cases. The improvement is not quite so good for the major axis: Although higher harmonics can reduce errors by factors of $\sim$2 or more, this often does not completely make up for the loss of precession, especially at 10° alignment. Errors in the measured spin behave similarly to the major axis—their measurement is improved, but not enough to fully compensate for the impact of aligned spins. By contrast, we find that higher harmonics *always* improve mass measurements beyond what can be done with random spins alone. In fact, partial alignment in many cases *improves* mass measurements, thanks to increased SNR in these cases.

We also briefly take a more detailed look at the relative improvement from spin precession, higher harmonics, and their combination. We confirm previous results that, for extrinsic parameters, the impact of the combined effects is not substantially greater than the impact of each effect alone. For mass errors, the higher harmonics dominate, with precession being almost irrelevant for the full waveform. For spin errors, however, the two effects do seem to be independent, with the combined improvement approximately equal to (or greater than) a simple multiplication of the individual improvements.

We conclude in Sec. V by summarizing our results and discussing additional studies that must be done before the question of LISA parameter estimation is fully understood. Throughout this paper, we use geometrized units in

which $G = c = 1$. A useful conversion factor is that $1M_\odot = 4.91 \times 10^{-6}$ s $= 1.47$ km.

Since this paper was originally written, budget constraints have caused a rescoping of the LISA mission, and the mission that eventually flies may differ from the ''classic'' configuration considered here. We continue to focus our analysis on measurements using LISA Classic for two reasons. First, the design of the rescoped mission is in flux. Until a design is fixed and its associated sensitivity known, we cannot study how well it will make measurements. Second, our goal is to make comparisons with previous studies that were based on the classic design. As such, it is most appropriate for us to use this design as well. We note that our conclusions should be robust in the sense that the general trends we find regarding the impact of spins and higher harmonics will be relevant to any LISA-like design (at least for designs that have five or six links, so both waveform polarizations can be simultaneously measured).

II. PARAMETER ESTIMATION CODE

The code used in this paper is a version of the MONTANA-MIT code used by the LISA Parameter Estimation Taskforce [34], updated with some new features and bug fixes.[3] In this section, we describe the relevant features of the code, especially how it differs from the code of Paper I [9]. We refer the reader to Paper I for more detailed discussion of the waveform and parameter estimation theory.

A. Massive black hole binary waveform

The waveform from a massive black hole binary coalescence is traditionally divided into three distinct phases: (1) the *inspiral* of the two holes, which can be described by the post-Newtonian expansion of general relativity; (2) the *merger* of the two holes into a common event horizon, describable only by full numerical relativistic simulations; and (3) the *ringdown* of the final hole into the stationary Kerr solution, which can be described by black hole perturbation theory. In this work, we consider only the inspiral, which for LISA sources can last for months to years, accumulating large amounts of SNR and parameter information. Because of this fact, as well as the ease of using the post-Newtonian approximation, inspiral-only waveforms have traditionally been used in most, though not all, LISA parameter estimation studies. Ringdown information was first studied on its own by Berti, Cardoso, and Will [8]. More recently, McWilliams *et al.* added both the merger and ringdown to the inspiral, albeit for nonspinning binaries with an *a priori* known mass ratio [17,19]. They showed that the merger can add a significant amount of parameter information, about a factor of 3 improvement in measurement accuracy for all parameters but mass. Work in progress will consider the impact of an unknown mass ratio, as well as spins.

The inspiral waveform can be described by 17 parameters: the masses of the black holes, m_1 and m_2; their dimensionless spins, $\chi_1 = |\mathbf{S}_1|/m_1^2$ and $\chi_2 = |\mathbf{S}_2|/m_2^2$; the spin angles at some particular reference time t_0, $\cos\theta_{S_1}(t_0)$, $\cos\theta_{S_2}(t_0)$, $\phi_{S_1}(t_0)$, and $\phi_{S_2}(t_0)$; the orientation angles of the orbital angular momentum at t_0, $\cos\theta_L(t_0)$ and $\phi_L(t_0)$; the eccentricity e; the periastron angle γ; the position of the binary on the sky, $\cos\theta_N$ and ϕ_N; the luminosity distance D_L; a reference time $t_{\rm ref}$ (possibly different from t_0); and a reference phase $\Phi_{\rm ref} = \Phi(t_{\rm ref})$. In this work, we assume quasicircular orbits, eliminating e and γ and reducing the parameter set to 15. This assumption is also quite common, since radiation reaction has long been expected to circularize binaries [35]. It should be noted, however, that recent studies indicate that gas [36,37] and/or stellar interactions [38] may cause binaries to retain a small, but significant, residual eccentricity when they enter the LISA band. Recent work by Key and Cornish [18] investigates the impact of this residual eccentricity using a nontrivial extension of our code.

In Paper I, we used the post-Newtonian parameters t_c and ϕ_c as the reference time $t_{\rm ref}$ and phase $\Phi_{\rm ref}$. These parameters are, respectively, the time and phase when the post-Newtonian frequency formally diverges. However, Paper I made a slight error in determining the post-Newtonian frequency and phase. To understand this error and how to correct it, begin with the time derivative of orbital angular frequency $\omega = 2\pi f_{\rm orb}$ (shown here to second post-Newtonian order)

$$\frac{d\omega}{dt} = \frac{96}{5}\frac{\eta}{M^2}(M\omega)^{11/3}\left[1 - \left(\frac{743}{336} + \frac{11}{4}\eta\right)(M\omega)^{2/3} + (4\pi - \beta)(M\omega) + \left(\frac{34103}{18144} + \frac{13661}{2016}\eta + \frac{59}{18}\eta^2 + \sigma\right)(M\omega)^{4/3}\right], \tag{2.1}$$

where $\eta = \mu/M$ is the reduced mass ratio, β is a spin-orbit coupling term, and σ is a spin-spin coupling term. Exact expressions for β and σ are given in Paper I. Equation (2.1) must be integrated once to obtain $\omega(t)$ and twice for the orbital phase $\Phi_{\rm orb}(t)$. When the spins do not precess, this integration can be done analytically to some specified post-Newtonian order. In Paper I, the analytic results were used, but with the time-dependent expressions for β and σ plugged in at the end of the process. This is technically not correct: The time-dependent spins should be inserted into (2.1), and then that expression should be numerically integrated to produce $\omega(t)$ and $\Phi_{\rm orb}(t)$. This is not difficult, only requiring two additional differential equations in the Runge-Kutta solver of Paper I. However, it means that t_c and Φ_c are no longer acceptable references,

[3] We note that the codes used in [34] were all found to produce the same answers provided they used the same noise models, the same signal cutoffs, and so on. Our code has been well-tested in as much as other codes had the same features to compare against.

since the numerical integrator cannot reach infinite frequency. We describe our current approach momentarily.

Another change from the code used in Paper I is in the choice of cutoff frequency for the inspiral. In Paper I, the inspiral was stopped at the frequency of the Schwarzschild innermost stable circular orbit (ISCO), $r = 6M$. This assumption is poor for two reasons. First, while $r = 6M$ is the ISCO for a test particle orbiting a single Schwarzschild hole of mass M, the dynamics of the two-hole system are much more complex, and the transition to plunge and merger is not so well-defined. Second, we are considering Kerr black holes, for which even in the point-particle limit the innermost stable orbit can vary from $r = 9M$ to $r = M$ depending on the spin of the hole, with a concomitantly wide variation in the ISCO frequency. A better solution is to stop the inspiral at the minimum energy circular orbit (MECO), the orbit which minimizes the expression for post-Newtonian energy [39]:

$$\begin{aligned} E = &-\frac{\mu}{2}(M\omega)^{2/3}\Bigg(1-\frac{1}{12}(9+\eta)(M\omega)^{2/3} \\ &+\frac{8}{3M^2}\Bigg[\left(1+\frac{3}{4}\frac{m_2}{m_1}\right)\hat{\mathbf{L}}\cdot\mathbf{S}_1+\left(1+\frac{3}{4}\frac{m_1}{m_2}\right)\hat{\mathbf{L}}\cdot\mathbf{S}_2\Bigg](M\omega) \\ &+\Bigg[\frac{1}{24}(-81+57\eta-\eta^2) \\ &+\frac{1}{\eta M^4}(\mathbf{S}_1\cdot\mathbf{S}_2-3(\hat{\mathbf{L}}\cdot\mathbf{S}_1)(\hat{\mathbf{L}}\cdot\mathbf{S}_2))\Bigg](M\omega)^{4/3}\Bigg). \end{aligned} \tag{2.2}$$

The MECO is known to be a better approximation to the inspiral-plunge transition than the ISCO, and it properly takes spins into account.

Using the MECO gives us a better reference point for our time and phase than the coalescence time and phase t_c and Φ_c described above. We choose $t_0 = t_{\rm ref} = t_{\rm MECO}$ and $\Phi_{\rm ref} = \Phi_{\rm MECO}$ and then integrate the spin, frequency, and phase evolution equations *backwards* from the MECO to $t = 0$. The backwards integration provides stability in the Fisher-matrix calculation: We align the waveforms when they are largest, thus making it easier to introduce slight perturbations.

As seen in Eq. (2.1), we calculate the phase out to second post-Newtonian (2PN) order. (By numerically integrating (2.1) to obtain $\omega(t)$ and $\Phi_{\rm orb}(t)$, we specifically are choosing the "TaylorT4" PN approximant [40].) We integrate the spin precession equations out to 1.5PN order, which includes 1PN spin-orbit and 1.5PN spin-spin terms. It is worth noting that all of the relevant quantities are known to higher post-Newtonian order. Work in preparation shows that including terms beyond the order we include here only causes a slight quantitative change in the accuracy with which parameters are measured [41]. In Sec. III, we use the restricted post-Newtonian approximation, in which we only consider the quadrupole term ($\Phi = 2\Phi_{\rm orb}$) with its lowest order, Newtonian amplitude. In Sec. IV, we use the full post-Newtonian waveform, which includes all harmonics to 2PN order in amplitude.

B. LISA response and noise

The LISA response used in this paper differs from the response used in Paper I. For signals which do not reach above 3×10^{-3} Hz, we use the same low-frequency approximation used in that paper. In this approximation, we ignore the transfer functions which arise due to the finite arm lengths of the detector. This approximation is very inaccurate above $f \sim 3 \times 10^{-3}$ Hz. With the addition of higher harmonics, many signals now reach into this range where the transfer functions become important.

The full LISA detector response is somewhat complicated to model. Three existing codes provide the full response: the LISA Simulator [42], Synthetic LISA [43], and LISACode [44]. Interfacing with one of these codes would significantly slow our analysis, making it difficult to perform large Monte Carlo studies over our parameter space. We seek a simpler response function which includes the finite arm length transfer functions but ignores some of the more complicated issues.

The three LISA spacecraft follow eccentric orbits around the Sun at 1 AU. The individual orbits combine in such a way that the LISA constellation maintains, at first order in orbital eccentricity, an equilateral triangle formation. By going beyond this leading order, one finds that the arm lengths vary by a small amount on monthlong time scales. The variation in LISA arm lengths is the reason for the development of time delay interferometry (TDI) techniques [45] to eliminate laser phase noise, which cancels exactly in equal-arm interferometers like LIGO. In our detector model, we approximate the constellation as having arm lengths that are equal at all times. Our model detector is a "rigid" equilateral triangle.

The other complexity in the full LISA response is that the spacecraft move during the measurement, causing "-point-ahead" effects which must be taken into account. We assume instead an "adiabatic" detector, in which for each time that we require the detector response, the detector is considered to be motionless for that time. The spacecraft then adiabatically move to their next position for the next sample point. This rigid, adiabatic approximation is known to be equivalent to the full response up to very high frequency (~ 500 mHz) and thus is appropriate for our Fisher-matrix analysis [42].

For the rigid, adiabatic approximation, the code produces Michelson variables X, Y, and Z as defined in [43], Eqs. (10) and (11). Note that these are technically *not* TDI variables. Since we do not have to subtract phase noise, there is no need to include another pass through the interferometer (cf. the "real" TDI variables in Eq. (13) of [43]). They do contain the same information, though, so we may refer to them as (pseudo, equal-arm) TDI Michelson variables in this paper. From them, we can construct noise-orthogonal TDI variables A, E, and T, defined as

$$A = \frac{1}{3}(2X - Y - Z), \tag{2.3}$$

$$E = \frac{1}{\sqrt{3}}(Z - Y), \tag{2.4}$$

$$T = \frac{1}{3}(X + Y + Z). \tag{2.5}$$

A, E, and T are used to calculate the SNR and the Fisher matrix. Note that, as defined in Eqs. (10) and (11) of [43], these are *fractional-frequency* variables. We can convert them to *equivalent strain* by integrating the signal in the frequency domain and then multiplying by $c/(4\pi L)$. For the low-frequency case, we use the Michelson signal X and the noise-orthogonal signal $(X + 2Y)/\sqrt{3}$. These combinations are denoted h_I and h_{II} in Paper I (which in turn follows the convention of Cutler [3]). The low-frequency approximation is constructed so that these signals are already expressed as equivalent strain.

The LISA noise power spectral density $S_n(f)$ comprises two parts, instrumental noise and confusion noise due to unresolved white dwarf binaries in the Galaxy. Instrumental noise consists of both position noise, due to photon shot noise and other effects along the optical path, and acceleration noise, due to proof mass motion. The total instrument noise in the A and E (strain) channels is given by

$$S_{n,AE} = \frac{1}{3L^2}\left[(2 + \cos x)S_p(f) + (1 + \cos x + \cos^2 x) \times \left(\frac{4S_a(f)}{(2\pi f)^4}\left[1 + \left(\frac{10^{-4}\ \mathrm{Hz}}{f}\right)\right]\right)\right], \tag{2.6}$$

and the T (strain) noise is given by

$$S_{n,T} = \frac{1}{3L^2}\left[(1 - \cos x)S_p(f) + \frac{1}{2}(1 - \cos x)^2\left(\frac{4S_a(f)}{(2\pi f)^4}\left[1 + \left(\frac{10^{-4}\,\mathrm{Hz}}{f}\right)\right]\right)\right]. \tag{2.7}$$

Here $L = 5 \times 10^9$ km is the LISA arm length, $x = 2\pi f L/c$, $S_p(f) = 3.24 \times 10^{-22}\ \mathrm{m}^2/\mathrm{Hz}$ is the position noise budget, and $S_a(f) = 9 \times 10^{-30}\ \mathrm{m}^2/\mathrm{s}^4/\mathrm{Hz}$ is the acceleration noise budget. For the low-frequency approximation, we can calculate similar expressions for the two noise-orthogonal channels and then take $\cos x = 1$, although this attention to detail makes little difference for the frequencies of interest. Notice that the position noise and acceleration noise are both assumed to be white, with no frequency dependence. However, because it is expected that LISA's acceleration noise performance will degrade somewhat from this white form below 10^{-4} Hz, we have also added a "pink" acceleration noise term, with a slope of f^{-1}.

Confusion noise is constructed from the residuals of a fit to the Galaxy [46] in the Mock LISA Data Challenge [22]. An approximate analytic expression for the confusion noise can be found in [18], Eq. (10). It is added to instrument noise for the A and E channels (or the orthogonal low-frequency channels) to obtain the total noise. It is not added to the T channel because it occurs only at low frequency, where that channel adds nothing to the analysis.

Finally, although it is not expressed explicitly in (2.6) and (2.7), we enforce a low-frequency cutoff of 3×10^{-5} Hz and do not include any contribution from the signal below that frequency in our analysis. (This frequency is the lowest frequency at which LISA is planned to have good sensitivity to gravitational waves; though it will have sensitivity to sources at lower frequencies, the noise characteristics below $f = 3 \times 10^{-5}$ Hz cannot be guaranteed.)

C. Construction of the Fisher matrix

The Fisher matrix Γ_{ij} is defined as

$$\Gamma_{ij} = \left(\frac{\partial h}{\partial \theta^i}\,\middle|\,\frac{\partial h}{\partial \theta^j}\right), \tag{2.8}$$

where h is the gravitational wave signal, θ^i are the 15 parameters which describe it, and

$$(a|b) = 4\,\mathrm{Re}\int_0^\infty df\,\frac{\tilde{a}^*(f)\tilde{b}(f)}{S_n(f)} \tag{2.9}$$

is a noise-weighted inner product. The inverse of the Fisher matrix is the covariance matrix, which contains squared parameter errors along the diagonal and correlations elsewhere. To calculate the Fisher matrix, we need the waveforms in the frequency domain. In Paper I, we actually did all calculations in the frequency domain by using the stationary phase approximation. This approximation relies on a separation of time scales and is known to be quite good for nonspinning binaries, where the inspiral time scale T_{insp} is much larger than the orbital time scale T_{orb}. However, when precession is included in the waveform, an additional time scale T_{prec} comes into play, with $T_{\mathrm{insp}} > T_{\mathrm{prec}} > T_{\mathrm{orb}}$. We have seen that with precession, the stationary phase approximation tends to smooth out sharp features in the Fourier transform, potentially reducing the information content. The problem becomes worse as the impact of precession increases (i.e., with higher spin values, or for highly nonaligned spins and orbit). To avoid introducing any errors due to this approximation, we here calculate our waveforms in the time domain and then perform a fast Fourier transform (FFT) to bring them into the frequency domain.

This approach has two major limitations. First, it is much slower than the stationary phase approach, since we need to calculate many time samples to observe Nyquist sampling requirements and we then need to compute the (FFT). Second, the FFT assumes a periodic signal. Because we have a finite signal which looks much different at the end than at the beginning, we must introduce some kind of window in order to taper the signal to zero at the beginning and end. We use a Hann window (actually half a Hann window at each end of the signal). This window substantially reduces "ringing," or spectral leakage

problems. However, it also cuts out part of the signal. This is particularly unfortunate for the strongly chirping inspiral, since much of the signal power is contained in the last few cycles. By windowing the signal, we lose some of this power. This may cause our SNR and errors to be smaller and larger, respectively, than they would be for a "real," physical signal. The best solution to this problem would be to include the merger and ringdown portions of the signal, allowing it to fade to zero in a physical, not artificial, way. For now, we must simply accept the windowing as part of the definition of the (unphysical) inspiral-only waveform.

III. PARAMETER ESTIMATION IN PARTIALLY ALIGNED BINARIES: ONLY THE QUADRUPOLE HARMONIC

Here we describe the parameter estimation capabilities of LISA without including the influence of higher harmonics. In order to consider a wide range of LISA sources, we choose only three parameters explicitly, the two masses of the system and the luminosity distance. For the masses, we consider a variety of systems ranging in total mass from $2 \times 10^5 M_\odot$ to $2 \times 10^7 M_\odot$, with a mass ratio from 1–10. On the other hand, we consider only sources at $z = 1$, corresponding to a luminosity distance of 6.64 Gpc using our choice of cosmological parameters. Errors at other redshifts can be constructed using the errors at $z = 1$. We note that the results at masses m_1 and m_2 and redshift z' can be simply related to the results at masses $m_1(1 + z')/(1 + z)$ and $m_2(1 + z')/(1 + z)$ and redshift z. This is because all time scales in the system are derived from the masses. Since time scales are lengthened (frequencies shortened) by the cosmological redshift, a binary at higher redshift behaves like a binary at lower redshift but with a higher mass. The quantity $m(1 + z)$ is generally called the redshifted mass, where m is the mass measured locally at the rest frame of the binary. (When we quote masses in this paper, we always mean the *rest-frame* mass, remembering that when put into the waveform formulas of Paper I, they must be multiplied by $1 + z$.) The amplitude of the waves at redshift z' is decreased by a factor $\xi = D_L(z)/D_L(z')$ over the corresponding binary (i.e., the binary with the same redshifted mass) at redshift z. This increases the errors by $1/\xi$ over that corresponding signal.

The other 12 parameters of the system are generated essentially at random, with 1000 different Monte Carlo realizations. For example, $t_{\rm MECO}$ is chosen from within an assumed three-year mission time, meaning that some early binaries will have abnormally short signals for a given mass. Spin magnitudes are chosen uniformly between 0 and 1, and $\Phi_{\rm MECO}$ is chosen uniformly between 0 and 2π. Cosines of angles are chosen uniformly between -1 and 1, while longitudinal angles are chosen uniformly between 0 and 2π. In the case of random spins (as in Paper I), the procedure is then complete. In the case of partially aligned spins, the main focus of this paper, we use the randomly generated parameters to integrate the spin precession equations backwards from the MECO to $t = 0$. We assume that any alignment at $t = 0$ is solely due to gas. If either of the resulting spin-orbit angles is greater than the model's restriction (30° or 10°), we randomly select new spin orientation angles (at MECO) and try again. This procedure guarantees that all sources will have the desired amount of alignment at the start of the signal. However, our sample will include some sources ($\sim 30\%$) which move out of alignment by MECO. Since these sources generally precess more strongly than the others, they tend to improve the overall distribution of parameter errors, especially for spin magnitude.

Figure 1 shows a histogram of the Monte Carlo results for a binary with $m_1 = 10^6 M_\odot$ and $m_2 = 3 \times 10^5 M_\odot$. We show the major axis of the sky position error ellipse, $2a$, comparing the cases of randomly aligned spins to spins restricted to be aligned within 30° (for hot gas) and 10° (for cold gas) of the orbital angular momentum. We see that partial alignment of the spins and orbital angular momentum degrades LISA's localization capability. For the partially aligned cases, the shapes of the histograms resemble the strongly peaked "no precession" results of Paper I more than the roughly flat random-spin histogram. The medians of the distributions also increase: While randomly oriented binaries have a median major axis of 34.8 arcminutes, systems aligned within 30° have a median $2a$ of 62.3 arcminutes. For 10° alignment, this degrades further to 90.5 arcminutes. This is a factor of 2.6 degradation from the case of random alignment, just short of the factor ~ 3 improvement seen in Paper I when precession is introduced into the waveform model. In essence, by

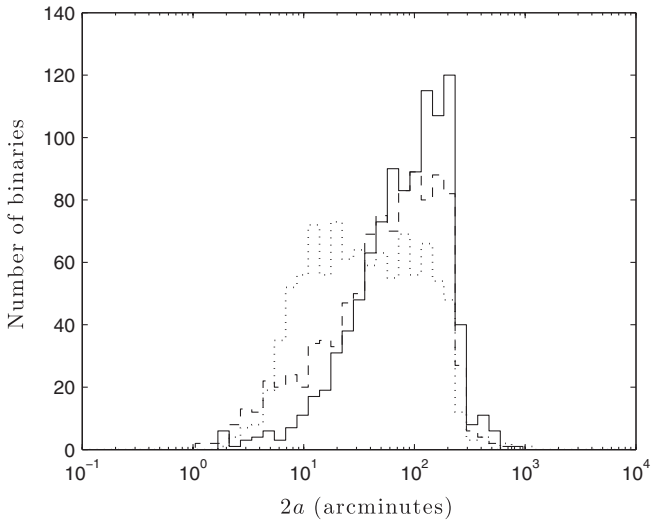

FIG. 1. Distribution of $2a$, the major axis of the sky position error ellipse, for binaries with randomly aligned spins (dotted line), spins restricted to within 30° of the orbital angular momentum (dashed line), and spins restricted to within 10° of the orbital angular momentum (solid line). Here $m_1 = 10^6 M_\odot$, $m_2 = 3 \times 10^5 M_\odot$, and $z = 1$.

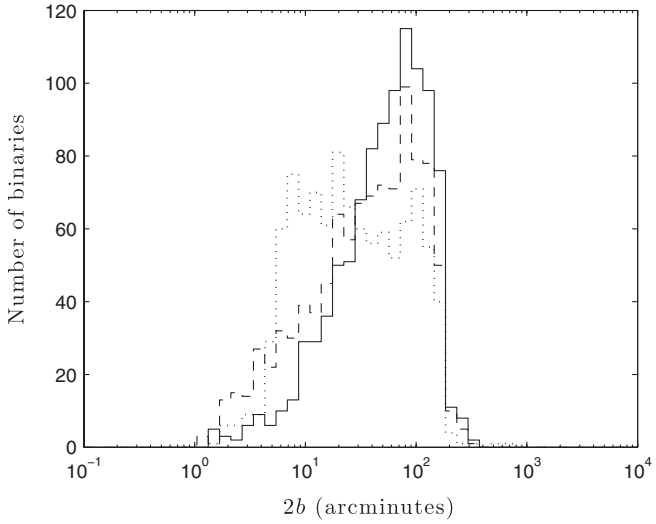

FIG. 2. Same as Fig. 1, but for the minor axis $2b$.

TABLE I. Median sky position major axis $2a$ and minor axis $2b$, in arcminutes, for binaries of various masses at $z = 1$, in the "no gas" (random-spin), "hot gas" (30° alignment), and "cold gas" (10° alignment) cases.

		No gas		Hot gas		Cold gas	
$m_1(M_\odot)$	$m_2(M_\odot)$	$2a$	$2b$	$2a$	$2b$	$2a$	$2b$
10^5	10^5	27.0	16.4	40.7	25.7	53.8	35.1
3×10^5	10^5	17.5	11.7	30.1	17.9	53.7	34.8
3×10^5	3×10^5	33.3	19.0	45.9	27.1	63.1	42.4
10^6	10^5	23.3	18.3	35.9	21.6	61.6	38.4
10^6	3×10^5	34.8	24.6	62.3	40.6	90.5	58.6
10^6	10^6	56.9	37.5	87.7	57.2	105	68.3
3×10^6	3×10^5	39.0	33.6	57.0	36.8	105	68.1
3×10^6	10^6	45.5	32.4	83.3	49.0	131	77.9
3×10^6	3×10^6	71.9	43.6	126	75.6	168	106
10^7	10^6	47.3	40.2	70.7	46.6	132	83.7
10^7	3×10^6	67.3	45.3	131	75.7	234	143
10^7	10^7	160	84.8	281	136	581	323

restricting the spin angles to within 10° of the orbital angular momentum, we have eliminated almost all of the advantage gained from including precession effects in the waveform.

Figure 2 shows results for the minor axis of the sky position error ellipse,[4] $2b$. The results are similar: The median value of $2b$ increases from 24.6 arcminutes for random spins to 40.6 arcminutes for 30° alignment and to 58.6 arcminutes for 10° alignment. Together with the results for the major axis, these numbers imply that the total sky position area increases by a factor >6 when binaries have closely aligned angular momentum vectors, strongly impacting the ability of LISA to find electromagnetic counterparts to the GW signal.

Table I shows the major and minor sky position axes for a range of masses, in the random-spin, hot gas, and cold gas cases. We see that degradation of a factor ~2–3 between the "no gas" and "cold gas" (10° alignment) cases occurs rather consistently for different masses and mass ratios.

The other extrinsic parameter of interest is the luminosity distance D_L. Figure 3 shows the fractional errors in D_L for different degrees of spin alignment. Again, we see that restricting the spin angles dramatically affects measurement: The median of 5.24×10^{-3} for random spin orientation doubles to 1.01×10^{-2} when the spins are aligned within 30° and nearly triples to 1.36×10^{-2} when the spins are aligned within 10°. However, this particular degradation is almost certainly immaterial, at least at low redshift, since the error remains much smaller than the ~5% error produced by weak gravitational lensing at $z\sim1$. For sources at higher redshift, this degradation may be more important. Table II shows luminosity distance errors for different masses. Like the sky position, the degradation is about a factor of ~1.5–2 for 30° alignment and ~2–3 for 10° alignment. Note that for the larger masses we consider, the degradation pushes the GW distance error to a value comparable to or even larger than the weak lensing error.

We now turn to the intrinsic parameters of the system, its masses and spins. Figs. 4 and 5 show the errors in the two black hole masses for the three cases we consider. Medians of $\Delta m_1/m_1$ are 4.84×10^{-3} for the random-spin case, 5.70×10^{-3} for a system with hot gas, and 8.23×10^{-3} for a system with cold gas. For $\Delta m_2/m_2$, these numbers are 3.84×10^{-3}, 4.54×10^{-3}, and 6.55×10^{-3}, respectively. The impact of partially aligned spins does not seem to be as strong on the masses as on the sky position; the mass errors change by less than a factor of 2. In Paper I, we looked at

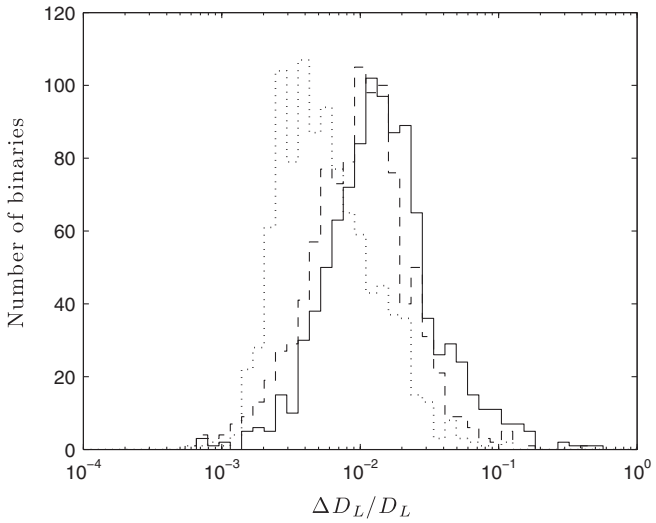

FIG. 3. Same as Fig. 1, but for the fractional error in luminosity distance, $\Delta D_L/D_L$.

[4]Note that unlike in Paper I, the results for $2b$ do not feature a long tail of small errors. We have confirmed that this effect was caused by a bug in the code used in Paper I.

TABLE II. Same as Table I, but for the fractional error in luminosity distance, $\Delta D_L/D_L$.

$m_1(M_\odot)$	$m_2(M_\odot)$	No gas	Hot gas	Cold gas
10^5	10^5	4.16×10^{-3}	7.97×10^{-3}	0.0130
3×10^5	10^5	2.59×10^{-3}	6.03×10^{-3}	0.0101
3×10^5	3×10^5	5.54×10^{-3}	9.23×10^{-3}	0.0121
10^6	10^5	3.67×10^{-3}	5.92×10^{-3}	0.0113
10^6	3×10^5	5.24×10^{-3}	0.0101	0.0136
10^6	10^6	9.37×10^{-3}	0.0137	0.0175
3×10^6	3×10^5	5.58×10^{-3}	9.19×10^{-3}	0.0147
3×10^6	10^6	7.06×10^{-3}	0.0130	0.0191
3×10^6	3×10^6	0.0137	0.0207	0.0279
10^7	10^6	7.67×10^{-3}	0.0135	0.0242
10^7	3×10^6	0.0129	0.0243	0.0429
10^7	10^7	0.0441	0.0613	0.0974

precession improvements not in individual masses but in chirp mass and reduced mass, where we saw factors of $\sim$10 and $\sim$100–1000 improvement, respectively. Clearly, restricting the spin directions does not remove this entire improvement; even a limited amount of precession appears to significantly aid mass determination. We can check this assertion using our new code by running a case with only 1° alignment between the spins and the orbit. We find that the 10° results improve on the 1° results by a factor of 3. By contrast, the sky position and distance errors differ by only 15–20%.

Table III shows the results for different masses. We see a much stronger dependence on mass ratio here than for the extrinsic parameters. For example, while the cold gas degradation is less than a factor of 2 for the (roughly) 3:1 mass ratio case considered in Figs. 4 and 5, it reaches a factor of $\sim$9 for the equal-mass case $m_1 = m_2 = 10^5 M_\odot$. This is unusual, since precession is known, at least for

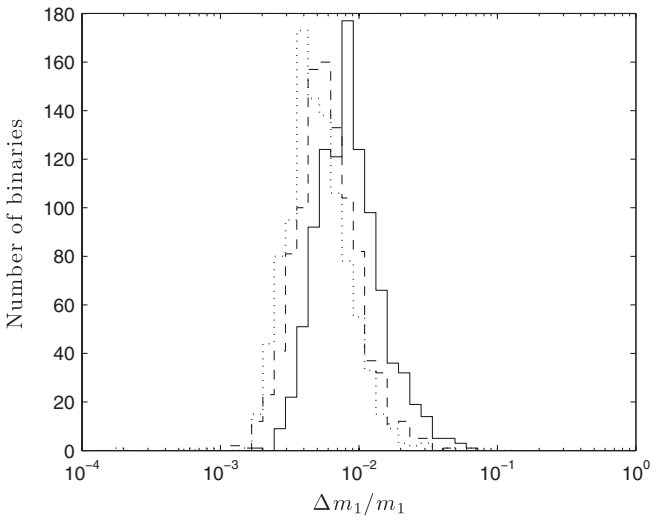

FIG. 4. Same as Fig. 1, but for the fractional error in mass, $\Delta m_1/m_1$.

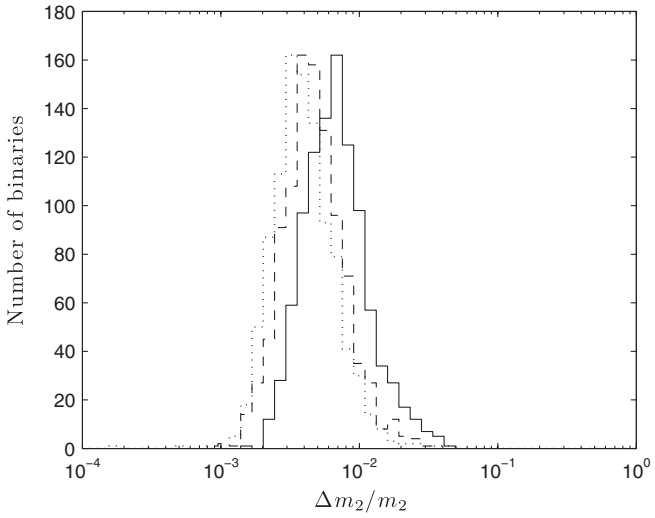

FIG. 5. Same as Fig. 1, but for the fractional error in mass, $\Delta m_2/m_2$.

extrinsic parameters, to have a stronger impact for unequal masses due to increased complexity in the signal. It is possible that the lack of this complexity essentially "gives away" that the masses are equal, making them easier to determine from the extremely well-measured chirp mass.

Interestingly, there are some examples of 10:1 mass ratio systems that break our general trend; in these cases, we find that partially aligned spins actually do better than random spins. This seemingly counterintuitive result can be explained by our choice of the minimum energy circular orbit (MECO) as the waveform cutoff. Binaries with aligned spins have a smaller MECO (with a corresponding high inspiral cutoff frequency) and thus accumulate more SNR than those with spins out of alignment (as many in the random-spin sample will be). Figure 6 shows the SNR for all three cases in a 10:1 binary. We see that the SNR is substantially larger for the partially aligned cases (medians of 2588 and 2592, for 30° and 10°, respectively) than the randomly aligned case (median of 1445). Even though these binaries precess less, the increase in SNR makes up for it in parameter estimation. It is worth noting that this effect could also be of use in detecting and measuring particularly high-mass binaries. For randomly chosen spins, such a binary might be mostly or completely out of the LISA band. However, if the spins are aligned by interactions with gas, the MECO frequency will be pushed into band.

Finally, we consider how restriction of spin angles affects measurement of spin magnitudes; Figs. 7 and 8 show these results. For χ_1, the median varies from 4.55×10^{-3} for no gas to 5.38×10^{-3} for hot gas to 1.31×10^{-2} for cold gas. For χ_2, the situation is similar; the medians are 1.48×10^{-2} (no gas), 1.72×10^{-2} (hot gas), and 5.11×10^{-2} (cold gas). Although the spin errors are degraded by partial alignment, the amount of degradation is somewhat

TABLE III. Same as Table I, but for the mass errors $\Delta m_1/m_1$ and $\Delta m_2/m_2$.

		No gas		Hot gas		Cold gas	
$m_1(M_\odot)$	$m_2(M_\odot)$	$\Delta m_1/m_1$	$\Delta m_2/m_2$	$\Delta m_1/m_1$	$\Delta m_2/m_2$	$\Delta m_1/m_1$	$\Delta m_2/m_2$
10^5	10^5	3.23×10^{-3}	3.24×10^{-3}	9.84×10^{-3}	9.84×10^{-3}	0.0284	0.0284
3×10^5	10^5	3.02×10^{-3}	2.45×10^{-3}	3.95×10^{-3}	3.20×10^{-3}	5.94×10^{-3}	4.83×10^{-3}
3×10^5	3×10^5	4.50×10^{-3}	4.50×10^{-3}	0.0129	0.0128	0.0327	0.0328
10^6	10^5	2.72×10^{-3}	1.90×10^{-3}	1.90×10^{-3}	1.32×10^{-3}	2.22×10^{-3}	1.55×10^{-3}
10^6	3×10^5	4.84×10^{-3}	3.84×10^{-3}	5.70×10^{-3}	4.54×10^{-3}	8.23×10^{-3}	6.55×10^{-3}
10^6	10^6	8.05×10^{-3}	8.05×10^{-3}	0.0197	0.0197	0.0475	0.0475
3×10^6	3×10^5	5.81×10^{-3}	4.01×10^{-3}	4.49×10^{-3}	3.07×10^{-3}	5.10×10^{-3}	3.51×10^{-3}
3×10^6	10^6	0.0121	9.73×10^{-3}	0.0165	0.0132	0.0233	0.0187
3×10^6	3×10^6	0.0239	0.0237	0.0536	0.0533	0.109	0.109
10^7	10^6	0.0176	0.0118	0.0167	0.0109	0.0205	0.0133
10^7	3×10^6	0.0431	0.0336	0.0581	0.0447	0.0924	0.0713
10^7	10^7	0.381	0.388	0.424	0.423	0.967	0.971

curbed by the contribution of binaries which precess away from alignment before MECO. In addition, the errors at 10° alignment are roughly an order of magnitude better than at 1° alignment. Similar to the situation with mass measurements, even a small amount of precession can have a huge impact on measuring spin.

Table IV gives spin errors for a broader range of masses. Like the mass errors, there is a strong dependence on mass ratio. In this case, however, the worst degradation occurs not for equal masses, but for 3:1 mass ratios, with factors of up to 4 increases in $\Delta\chi_1$ and factors of up to 6 increases in $\Delta\chi_2$. The 10:1 cases show some degradation at 10° alignment, but many cases are slightly improved at 30° alignment. As in the case of mass measurements (cf. Table III), this can be attributed to the increased SNR for aligned binaries.

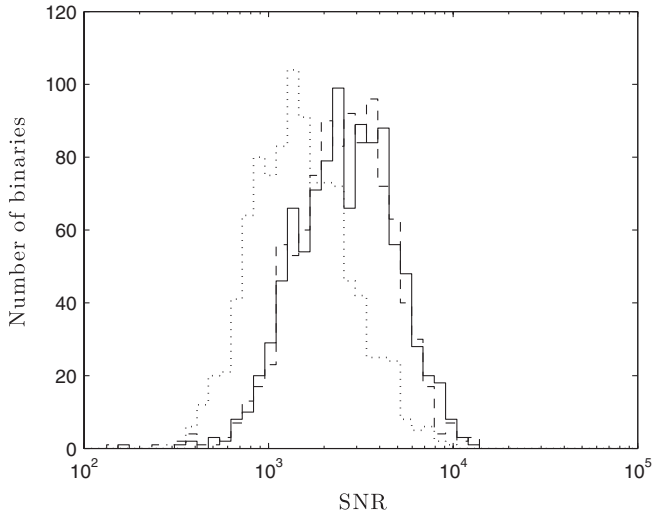

FIG. 6. Signal-to-noise ratio for binaries with randomly aligned spins (dotted line), spins restricted to within 30° of the orbital angular momentum (dashed line), and spins restricted to within 10° of the orbital angular momentum (solid line). Here $m_1 = 10^6 M_\odot$, $m_2 = 10^5 M_\odot$, and $z = 1$.

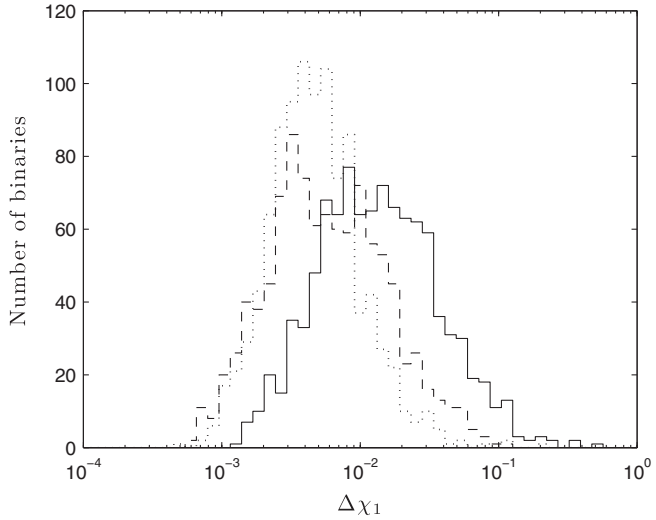

FIG. 7. Same as Fig. 1, but for the error in spin magnitude, $\chi_1 = |\mathbf{S}_1|/m_1^2$.

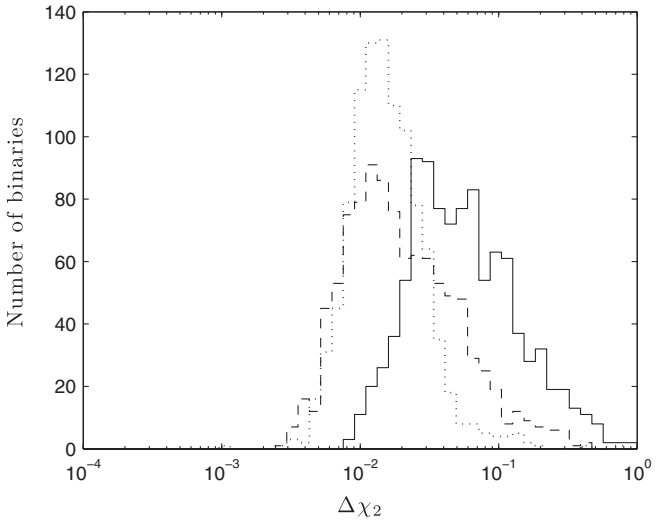

FIG. 8. Same as Fig. 1, but for the error in spin magnitude, $\chi_2 = |\mathbf{S}_2|/m_2^2$.

TABLE IV. Same as Table I, but for the spin magnitude errors $\Delta\chi_1$ and $\Delta\chi_2$.

		No gas		Hot gas		Cold gas	
$m_1(M_\odot)$	$m_2(M_\odot)$	$\Delta\chi_1$	$\Delta\chi_2$	$\Delta\chi_1$	$\Delta\chi_2$	$\Delta\chi_1$	$\Delta\chi_2$
10^5	10^5	0.0217	0.0210	0.0311	0.0310	0.0391	0.0388
3×10^5	10^5	3.18×10^{-3}	7.61×10^{-3}	4.98×10^{-3}	0.0155	0.0125	0.0467
3×10^5	3×10^5	0.0321	0.0315	0.0390	0.0382	0.0430	0.0417
10^6	10^5	1.30×10^{-3}	0.0355	1.05×10^{-3}	0.0225	2.22×10^{-3}	0.0358
10^6	3×10^5	4.55×10^{-3}	0.0148	5.38×10^{-3}	0.0172	0.0131	0.0511
10^6	10^6	0.0534	0.0505	0.0655	0.0645	0.0774	0.0753
3×10^6	3×10^5	2.38×10^{-3}	0.0601	1.70×10^{-3}	0.0499	3.24×10^{-3}	0.0659
3×10^6	10^6	9.92×10^{-3}	0.0186	0.0111	0.0264	0.0252	0.0787
3×10^6	3×10^6	0.134	0.125	0.197	0.198	0.234	0.232
10^7	10^6	4.86×10^{-3}	0.124	3.69×10^{-3}	0.180	7.03×10^{-3}	0.231
10^7	3×10^6	0.0266	0.0446	0.0298	0.0852	0.0652	0.191
10^7	10^7	1.69	1.54	1.28	1.31	1.86	1.87

IV. PARAMETER ESTIMATION IN PARTIALLY ALIGNED BINARIES: INCLUDING HIGHER HARMONICS

We now move beyond the leading quadrupole waveform to the full waveforms. Post-Newtonian corrections to the waveform amplitude are included up to 2PN order, including both additional quadrupole terms ($\Phi = 2\Phi_{\rm orb}$) and subleading ("higher") harmonics beyond the quadrupole. For example, the barycentric waveform $h_+(t)$ can be written up to 1PN order in the amplitude as

$$h_+(t) = \frac{2\mu x}{D_L}\Bigg\{(1+c_i^2)\cos 2\Phi_{\rm orb} + x^{1/2}\frac{s_i}{8}\frac{\Delta m}{M}[(5+c_i^2)\times\cos\Phi_{\rm orb} - 9(1+c_i^2)\cos 3\Phi_{\rm orb}] + x\Bigg[-\frac{1}{6}(19 + 9c_i^2 - 2c_i^4 - \eta(19 - 11c_i^2 - 6c_i^4))\cos 2\Phi_{\rm orb} + \frac{4}{3}s_i^2(1+c_i^2)(1-3\eta)\cos 4\Phi_{\rm orb}\Bigg]\Bigg\}, \quad (4.1)$$

where $x = (M\omega)^{2/3}$, $c_i = \cos(\hat{\mathbf{L}}\cdot\hat{\mathbf{n}})$, $s_i = \sin(\hat{\mathbf{L}}\cdot\hat{\mathbf{n}})$, and $\Delta m = m_1 - m_2$. Here we see both extra harmonics and a 1PN correction to the quadrupole harmonic. Note that the odd harmonics only contribute if $m_1 \neq m_2$; just like spin precession, higher harmonic corrections are more complex for unequal masses. Further terms (including the $\times$ polarization) can be found in [47] (albeit with some differences in sign convention).

It has been shown that higher harmonic corrections can improve parameter estimation much like spin precession does [10–12,14]. In the case of higher harmonics, degeneracies are broken due to the different sky position dependence of each harmonic. However, these studies did not include precession and so could not comment on how the two effects would combine. More recently, both effects were included in a parameter estimation study by Klein *et al.* (Ref. [16]). Their results demonstrate that including both precession and higher harmonics improves measurement accuracy, but, at least for extrinsic variables (sky position and distance), the combined improvement is not as drastic as the improvement from each effect on its own. This indicates that at least in some cases, precession and higher harmonics encode similar information. We might therefore expect that in partially aligned binaries for which spin precession exists but is suppressed, the inclusion of higher harmonics may make up for this suppression and restore much, if not all, of the lost parameter estimation capability. In this section, we test that expectation.

Figure 9 shows the major axis of the sky position error ellipse for the same binaries as Fig. 1, except with higher

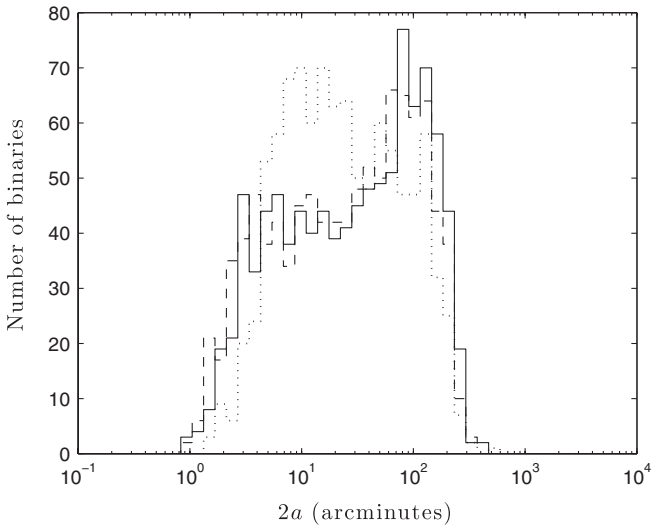

FIG. 9. Distribution of $2a$, the major axis of the sky position error ellipse, for binaries with randomly aligned spins (dotted line), spins restricted to within 30° of the orbital angular momentum (dashed line), and spins restricted to within 10° of the orbital angular momentum (solid line). Here $m_1 = 10^6 M_\odot$, $m_2 = 3\times10^5 M_\odot$, and $z = 1$. Higher harmonics are now included in the waveform model.

harmonics now added to the waveform model. The median value of $2a$ for random-spin, gas-free systems is 21.7 arcminutes. Comparing to the leading quadrupole waveform value of 34.8 arcminutes, we see that higher harmonics do indeed add some additional information not contained in precession. The difference between the two values is a factor ~ 1.6, consistent with the results of [16]. For partially aligned systems, the shape of the plot shows that the higher harmonics have had an important effect; both partially aligned histograms look much more like the roughly flat random-spin case than the strongly peaked histograms shown in Fig. 1. The median is 28.2 arcminutes for hot gas and 32.7 arcminutes for cold gas. Both results are great improvements on the leading quadrupole waveform values (factors ~ 2.2 and 2.8, respectively), indicating that the inclusion of higher harmonics has indeed "made up" for the loss of some spin precession. Both results are actually *better* than the leading quadrupole, gas-free result of 34.8 arcminutes. In this case, a full waveform with a small amount of precession does better than a leading quadrupole waveform with potentially significant precession.

Figure 10 shows the results for the minor axis $2b$, with medians 16.1 arcminutes for random spins and 13.7 arcminutes for both 30° and 10° alignment. These are all better than the leading quadrupole, random-spin result of 24.6 arcminutes. More interestingly, we see that when higher harmonics are included, the "cold gas" and "hot gas" errors are smaller than the "no gas" errors. As discussed in the previous section, this is due to the improvement in SNR in the aligned case. Higher harmonics break degeneracies well enough that it is more beneficial to have partially aligned binaries with more SNR and less precession than randomly aligned binaries with less SNR and more precession.

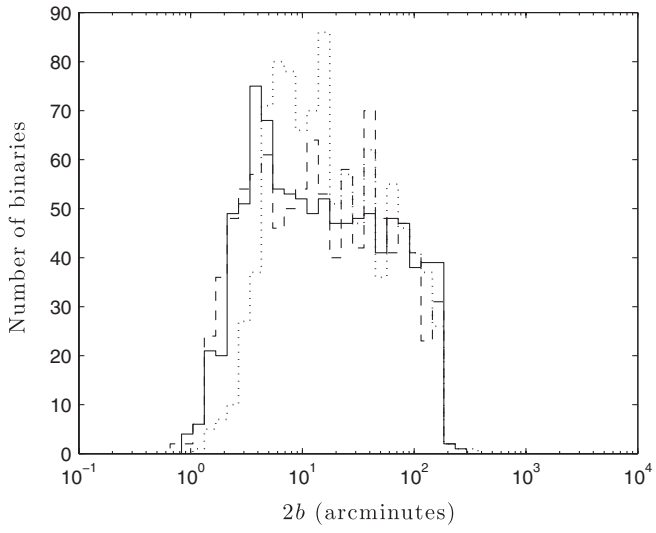

FIG. 10. Same as Fig. 9, but for the minor axis $2b$.

TABLE V. Median sky position major axis $2a$ and minor axis $2b$, in arcminutes, for binaries of various masses at $z = 1$, in the "no gas" (random-spin), "hot gas" (30° alignment), and "cold gas" (10° alignment) cases when higher harmonics are included in the waveform model. **Bold** entries are those that do better than the no gas case when higher harmonics are ignored (i.e., Table I). *Italic* entries do worse than that case, but only by 10% or less.

		No gas		Hot gas		Cold gas	
$m_1(M_\odot)$	$m_2(M_\odot)$	$2a$	$2b$	$2a$	$2b$	$2a$	$2b$
10^5	10^5	**21.8**	**12.3**	30.3	**14.2**	35.6	**15.9**
3×10^5	10^5	**14.3**	**9.67**	19.9	**10.1**	31.0	13.2
3×10^5	3×10^5	**26.2**	**16.2**	**30.4**	**18.3**	39.1	25.6
10^6	10^5	**14.0**	**11.9**	**13.7**	**9.25**	**17.6**	**9.69**
10^6	3×10^5	**21.7**	**16.1**	**28.2**	**13.7**	**32.7**	**13.7**
10^6	10^6	**48.1**	**32.0**	*60.4*	**37.1**	**53.0**	**32.4**
3×10^6	3×10^5	**29.1**	**25.8**	**25.7**	**20.0**	**35.8**	**24.4**
3×10^6	10^6	**36.0**	**26.8**	*48.2*	**27.4**	58.2	**30.2**
3×10^6	3×10^6	**63.5**	**39.8**	103	58.1	109	66.5
10^7	10^6	**36.7**	**32.4**	**38.9**	**27.4**	54.7	**31.3**
10^7	3×10^6	**45.0**	**32.8**	**65.1**	**33.0**	82.7	**36.5**
10^7	10^7	**114**	**65.6**	**144**	**80.1**	228	115

Table V shows results for a variety of masses. All show improvement from Table I; however, the improvement is not always as strong as in the case discussed above ($m_1 = 10^6 M_\odot$, $m_2 = 3\times10^5 M_\odot$). Bold text indicates cases in which the errors match or improve upon the results from the leading quadrupole waveform for random spins. Italics indicate errors which are worse, but by no more than 10%. Because of statistical issues, these cases could very well be "bold" in a different Monte Carlo run, so we will consider them as such for purposes of summarizing the results. While hot gas (30° alignment) systems achieve this particular benchmark for a majority of mass cases, cold gas (10° alignment) systems do not. Cold gas systems do, however, meet it for a majority of mass cases if only the minor axis is considered; $2b$ generally fares better than $2a$. Both axes exhibit cases where errors are smaller with alignment than without, the minimum sometimes occurring in a "sweet spot" of 30° alignment and sometimes at 10° alignment. In general, errors are better for larger mass ratios. This is to be expected because both higher harmonics and precession have a more complicated structure for larger mass ratios. Finally, the improvements are worst for the smallest masses, where the higher harmonics (except the $\cos\Phi_{\rm orb}$ terms, which are technically "lower" harmonics) begin to go out of band.

Figure 11 shows the results for luminosity distance errors $\Delta D_L/D_L$. Here the medians are 3.20×10^{-3}, 3.20×10^{-3}, and 3.54×10^{-3} for the no gas, hot gas, and cold gas cases, respectively. Again, these are all better than the leading quadrupole, no gas value of 5.24×10^{-3}, as we might expect since distance determination is strongly tied to sky position determination. Table VI gives the results for various masses. Most cases beat the leading

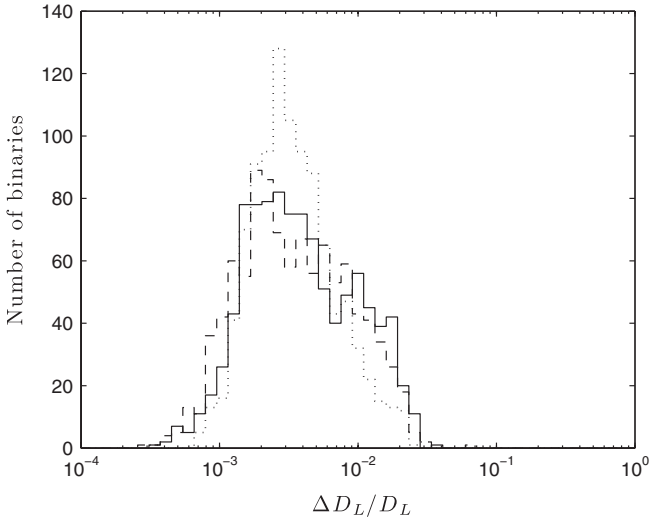

FIG. 11. Same as Fig. 9, but for the fractional error in luminosity distance, $\Delta D_L/D_L$.

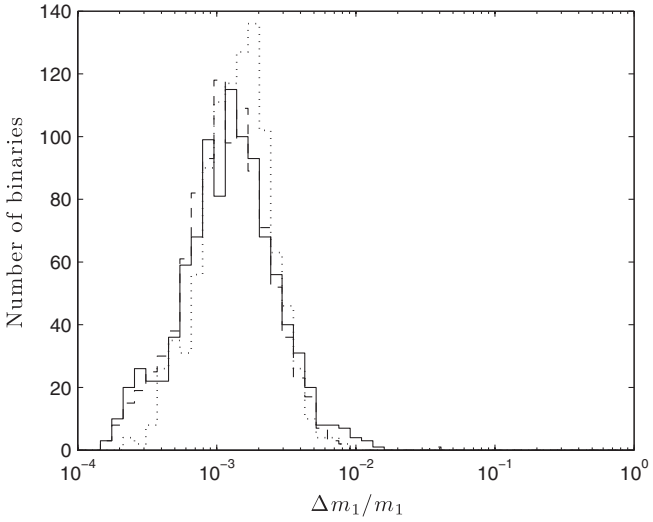

FIG. 12. Same as Fig. 9, but for the fractional error in mass, $\Delta m_1/m_1$.

quadrupole, no gas values of Table II or come within 10%. That is, except for the lowest mass systems, using the full waveform essentially always brings the distance errors for aligned spins back to the level of random spins. In this respect, distance errors are similar to (and even a bit better than) the minor axis of the sky position error ellipse. Finally, as with sky position, some mass cases feature errors which decrease as spins become aligned.

Figs. 12 and 13 show the results for masses m_1 and m_2. The medians for $\Delta m_1/m_1$ are 1.44×10^{-3} (no gas), 1.17×10^{-3} (hot gas), and 1.24×10^{-3} (cold gas). For $\Delta m_2/m_2$, these are 1.15×10^{-3} (no gas), 9.32×10^{-4} (hot gas), and 9.85×10^{-4} (cold gas). These are all significant improvements on the leading quadrupole, no gas case, about a factor of 3–4. It seems that for mass errors, higher harmonics are more useful than spin precession.

This conclusion is supported by Table VII. Here we see that every case is significantly improved over the leading quadrupole, random-spin result. The effect is strongest at higher masses, where the improvement can be an order of magnitude or more. This is due to the well-known effect of higher harmonics on higher mass signals: Normally these signals are only in band for a short amount of time. The inclusion of higher frequencies keeps the signal in band longer, allowing for the accumulation of more phase and better mass determination. The improvement is also greater for equal masses, similar to what was seen in Sec. III for precession.

While the extrinsic parameter errors were only occasionally reduced by partial alignment, this phenomenon occurs almost always for mass errors. This might be expected, since the effect showed up previously for mass errors (in Table III) even without higher harmonics to

TABLE VI. Same as Table V, but for the fractional error in luminosity distance, $\Delta D_L/D_L$.

$m_1(M_\odot)$	$m_2(M_\odot)$	No gas	Hot gas	Cold gas
10^5	10^5	$\mathbf{3.83 \times 10^{-3}}$	5.95×10^{-3}	7.23×10^{-3}
3×10^5	10^5	$\mathbf{1.89 \times 10^{-3}}$	2.88×10^{-3}	4.05×10^{-3}
3×10^5	3×10^5	$\mathbf{4.16 \times 10^{-3}}$	$\mathbf{4.78 \times 10^{-3}}$	$\mathbf{5.45 \times 10^{-3}}$
10^6	10^5	$\mathbf{2.07 \times 10^{-3}}$	$\mathbf{1.66 \times 10^{-3}}$	$\mathbf{2.12 \times 10^{-3}}$
10^6	3×10^5	$\mathbf{3.20 \times 10^{-3}}$	$\mathbf{3.20 \times 10^{-3}}$	$\mathbf{3.54 \times 10^{-3}}$
10^6	10^6	$\mathbf{7.16 \times 10^{-3}}$	$\mathbf{7.62 \times 10^{-3}}$	$\mathbf{7.48 \times 10^{-3}}$
3×10^6	3×10^5	$\mathbf{4.01 \times 10^{-3}}$	$\mathbf{3.29 \times 10^{-3}}$	$\mathbf{3.77 \times 10^{-3}}$
3×10^6	10^6	$\mathbf{5.38 \times 10^{-3}}$	$\mathbf{6.23 \times 10^{-3}}$	$\mathbf{6.79 \times 10^{-3}}$
3×10^6	3×10^6	**0.0115**	*0.0139*	0.0152
10^7	10^6	$\mathbf{5.69 \times 10^{-3}}$	$\mathbf{5.69 \times 10^{-3}}$	$\mathbf{7.42 \times 10^{-3}}$
10^7	3×10^6	$\mathbf{7.69 \times 10^{-3}}$	$\mathbf{9.02 \times 10^{-3}}$	**0.0121**
10^7	10^7	**0.0223**	**0.0270**	**0.0302**

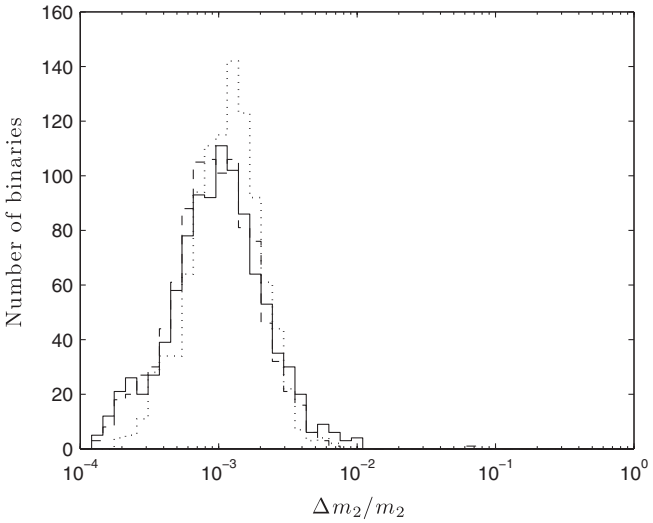

FIG. 13. Same as Fig. 9, but for the fractional error in mass, $\Delta m_2/m_2$.

TABLE VII. Same as Table V, but for the mass errors $\Delta m_1/m_1$ and $\Delta m_2/m_2$.

		No gas		Hot gas		Cold gas	
$m_1(M_\odot)$	$m_2(M_\odot)$	$\Delta m_1/m_1$	$\Delta m_2/m_2$	$\Delta m_1/m_1$	$\Delta m_2/m_2$	$\Delta m_1/m_1$	$\Delta m_2/m_2$
10^5	10^5	$\mathbf{1.22 \times 10^{-3}}$	$\mathbf{1.21 \times 10^{-3}}$	$\mathbf{1.16 \times 10^{-3}}$	$\mathbf{1.16 \times 10^{-3}}$	$\mathbf{1.24 \times 10^{-3}}$	$\mathbf{1.24 \times 10^{-3}}$
3×10^5	10^5	$\mathbf{1.29 \times 10^{-3}}$	$\mathbf{1.04 \times 10^{-3}}$	$\mathbf{1.43 \times 10^{-3}}$	$\mathbf{1.16 \times 10^{-3}}$	$\mathbf{1.77 \times 10^{-3}}$	$\mathbf{1.44 \times 10^{-3}}$
3×10^5	3×10^5	$\mathbf{6.14 \times 10^{-4}}$	$\mathbf{6.13 \times 10^{-4}}$	$\mathbf{5.37 \times 10^{-4}}$	$\mathbf{5.35 \times 10^{-4}}$	$\mathbf{5.12 \times 10^{-4}}$	$\mathbf{5.14 \times 10^{-4}}$
10^6	10^5	$\mathbf{1.32 \times 10^{-3}}$	$\mathbf{9.19 \times 10^{-4}}$	$\mathbf{9.23 \times 10^{-4}}$	$\mathbf{6.39 \times 10^{-4}}$	$\mathbf{1.10 \times 10^{-3}}$	$\mathbf{7.64 \times 10^{-4}}$
10^6	3×10^5	$\mathbf{1.44 \times 10^{-3}}$	$\mathbf{1.15 \times 10^{-3}}$	$\mathbf{1.17 \times 10^{-3}}$	$\mathbf{9.32 \times 10^{-4}}$	$\mathbf{1.24 \times 10^{-3}}$	$\mathbf{9.85 \times 10^{-4}}$
10^6	10^6	$\mathbf{1.27 \times 10^{-3}}$	$\mathbf{1.28 \times 10^{-3}}$	$\mathbf{7.64 \times 10^{-4}}$	$\mathbf{7.65 \times 10^{-4}}$	$\mathbf{7.25 \times 10^{-4}}$	$\mathbf{7.21 \times 10^{-4}}$
3×10^6	3×10^5	$\mathbf{2.50 \times 10^{-3}}$	$\mathbf{1.73 \times 10^{-3}}$	$\mathbf{1.47 \times 10^{-3}}$	$\mathbf{1.00 \times 10^{-3}}$	$\mathbf{1.62 \times 10^{-3}}$	$\mathbf{1.12 \times 10^{-3}}$
3×10^6	10^6	$\mathbf{3.06 \times 10^{-3}}$	$\mathbf{2.45 \times 10^{-3}}$	$\mathbf{2.55 \times 10^{-3}}$	$\mathbf{2.05 \times 10^{-3}}$	$\mathbf{2.65 \times 10^{-3}}$	$\mathbf{2.13 \times 10^{-3}}$
3×10^6	3×10^6	$\mathbf{2.04 \times 10^{-3}}$	$\mathbf{2.03 \times 10^{-3}}$	$\mathbf{1.48 \times 10^{-3}}$	$\mathbf{1.48 \times 10^{-3}}$	$\mathbf{1.47 \times 10^{-3}}$	$\mathbf{1.47 \times 10^{-3}}$
10^7	10^6	$\mathbf{4.52 \times 10^{-3}}$	$\mathbf{3.04 \times 10^{-3}}$	$\mathbf{3.17 \times 10^{-3}}$	$\mathbf{2.08 \times 10^{-3}}$	$\mathbf{3.55 \times 10^{-3}}$	$\mathbf{2.35 \times 10^{-3}}$
10^7	3×10^6	$\mathbf{4.04 \times 10^{-3}}$	$\mathbf{3.12 \times 10^{-3}}$	$\mathbf{3.56 \times 10^{-3}}$	$\mathbf{2.73 \times 10^{-3}}$	$\mathbf{4.21 \times 10^{-3}}$	$\mathbf{3.28 \times 10^{-3}}$
10^7	10^7	$\mathbf{5.05 \times 10^{-3}}$	$\mathbf{4.90 \times 10^{-3}}$	$\mathbf{4.17 \times 10^{-3}}$	$\mathbf{4.01 \times 10^{-3}}$	$\mathbf{4.50 \times 10^{-3}}$	$\mathbf{4.18 \times 10^{-3}}$

help break degeneracies. In general, the difference in mass accuracy between gas environments is relatively small. Partial alignment of spins does not affect mass determination as long as the signal model includes higher harmonics; such alignment may even help measure mass, at least slightly.

Finally, Figs. 14 and 15 present the errors in spin magnitude. These figures clearly show that higher harmonics do *not* help spin errors as much as spin precession does. This is to be expected, as the spin magnitudes drive the precession but do not appear in the higher harmonic amplitudes. Any gain in spin accuracy due to higher harmonics is a result of improvement in other parameters (such as the masses) which are correlated with the spins. For χ_1, the median errors are 2.20×10^{-3} for no gas, 3.01×10^{-3} for hot gas, and 6.88×10^{-3} for cold gas; for χ_2, these numbers are 1.21×10^{-2}, 1.45×10^{-2}, and 3.33×10^{-2}. While these errors represent improvements (up to a factor of ~ 2) over their leading quadrupole waveform counterparts, it is worth noting that for this "fiducial" case, spins are the only parameters for which the cold gas errors with higher harmonics do not improve upon the no gas errors for the leading quadrupole waveform. (Recall, however, that for other masses, sky position and distance errors do not always achieve this benchmark.) Table VIII shows the results for various masses. The cold gas error only beats the no gas, leading quadrupole error in a few cases.

We conclude this section by looking more directly at the impact of different degeneracy-breaking effects on parameter errors. Figure 16 shows multiplicative improvement factors (i.e., ratios of errors) when either precession, harmonics, or both effects are included in the waveform. For this purpose, we consider binaries with 10° alignment to represent "no precession" and those with random spins to represent "precession." (Remember, though, that even 10° alignment permits enough precession to significantly

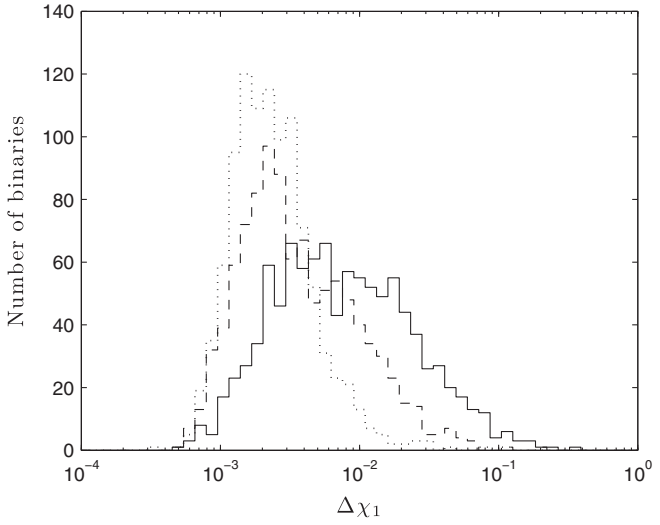

FIG. 14. Same as Fig. 9, but for the error in spin magnitude, $\chi_1 = |\mathbf{S}_1|/m_1^2$.

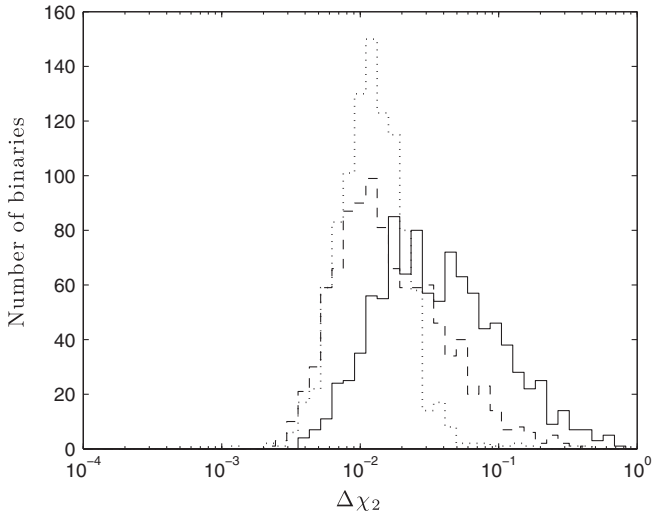

FIG. 15. Same as Fig. 9, but for the error in spin magnitude, $\chi_2 = |\mathbf{S}_2|/m_2^2$.

TABLE VIII. Same as Table V, but for the spin magnitude errors $\Delta\chi_1$ and $\Delta\chi_2$.

		No gas		Hot gas		Cold gas	
$m_1(M_\odot)$	$m_2(M_\odot)$	$\Delta\chi_1$	$\Delta\chi_2$	$\Delta\chi_1$	$\Delta\chi_2$	$\Delta\chi_1$	$\Delta\chi_2$
10^5	10^5	**0.0155**	**0.0157**	**0.0178**	**0.0178**	0.0286	0.0280
3×10^5	10^5	**1.79×10^{-3}**	**6.18×10^{-3}**	**3.09×10^{-3}**	0.0118	7.03×10^{-3}	0.0275
3×10^5	3×10^5	**0.0207**	**0.0211**	**0.0247**	**0.0243**	*0.0335*	*0.0335*
10^6	10^5	**6.43×10^{-4}**	**0.0196**	**6.21×10^{-4}**	**0.0137**	1.61×10^{-3}	**0.0263**
10^6	3×10^5	**2.20×10^{-3}**	**0.0121**	**3.01×10^{-3}**	**0.0145**	6.88×10^{-3}	0.0333
10^6	10^6	**0.0311**	**0.0326**	**0.0385**	**0.0396**	0.0603	0.0590
3×10^6	3×10^5	**1.07×10^{-3}**	**0.0373**	**8.64×10^{-4}**	**0.0218**	**2.24×10^{-3}**	**0.0408**
3×10^6	10^6	**3.90×10^{-3}**	**0.0153**	**5.29×10^{-3}**	0.0221	0.0129	0.0551
3×10^6	3×10^6	**0.0664**	**0.0669**	**0.0932**	**0.0899**	0.172	0.171
10^7	10^6	**1.75×10^{-3}**	**0.0552**	**1.67×10^{-3}**	**0.0482**	**4.03×10^{-3}**	**0.0872**
10^7	3×10^6	**6.03×10^{-3}**	**0.0295**	**0.0111**	0.0557	**0.0264**	0.140
10^7	10^7	**0.495**	**0.525**	**0.548**	**0.581**	**1.08**	**1.08**

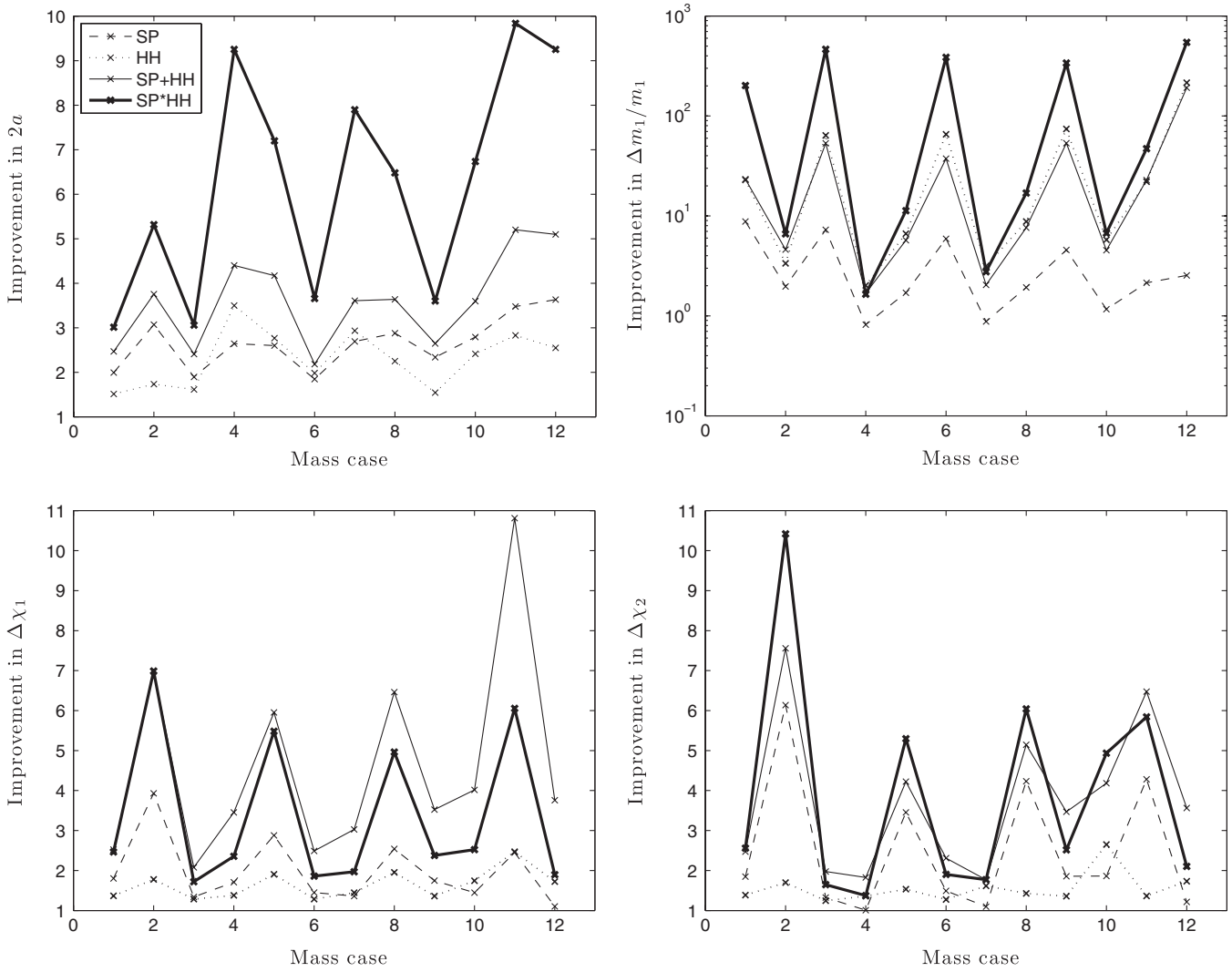

FIG. 16. Factors by which measurement accuracy improves for different parameters when various degeneracy-breaking effects are included in the signal: spin precession (SP), higher harmonics (HH), and both (SP + HH). We also show the product of the individual precession and harmonic improvements (SP*HH); this represents the naive limit by which the two effects would improve measurement accuracy if their individual improvements simply combined. Each point represents one of the 12 mass cases, arranged in order from left to right as they read top to bottom in Tables I, II, III, IV, V, VI, VII, and VIII.

impact mass and spin estimation.) We also show the product of the individual improvements from precession and harmonics. This naive limit describes how the improvements would combine if each effect were completely uncorrelated from the other.

For extrinsic parameters (represented in the figure by $2a$; results for $2b$ and D_L are very similar), the results confirm what was known previously. While including both precession and harmonics improves errors more than one effect alone, the total improvement falls well short of the naive expectation. In essence, a degeneracy can only be broken once. For mass (shown on a log scale), the same is true, but with the special feature pointed out above: Once harmonics are included, they essentially dominate mass accuracy determination. Spin precession is then a small liability, because the associated misaligned spins reduce SNR. For spin errors, on the other hand, the combined improvement due to both effects *does* roughly match the naive expectation. In the case of χ_1, the improvement is actually greater than the product of the individual improvements. Different behavior for spin magnitudes is to be expected, since the information about spin contained in harmonics is very indirect. This information is therefore independent of any information derived directly from precession.

V. CONCLUSIONS

Past work has shown that both spin precession and higher harmonics improve LISA's ability to measure the parameters of merging massive black hole binaries. Though these two effects produce similar degeneracy-breaking effects and similar improvements to measurement errors, there is one key difference between the two: Higher harmonics are *always* present in the signal (although the strength of odd harmonics depends on mass ratio). Spin precession, on the other hand, may be highly attenuated for *physical* reasons, namely, the partial alignment of spins due to interaction with gas. In this paper, we have studied how this partial alignment affects parameter measurement errors.

Initially ignoring the impact of higher harmonics, we found that sky position and distance are measured a factor of $\sim$1.5–2 less accurately for systems aligned within 30° (due to hot gas) and $\sim$2–3 less accurately for systems aligned within 10° (due to cold gas). A degradation of $\sim$3 would correspond to an order of magnitude decrease in LISA's ability to localize a source on the sky and a half order of magnitude decrease in the ability to localize it in redshift space. Since systems with gas, whether hot or cold, are the most likely to produce electromagnetic counterparts, this means that the results of Paper I and [13,15] strongly overestimate our ability to find these counterparts. Mass and spin measurements are also degraded by spin alignment, in some cases by factors up to $\sim$9. However, because the masses and spins are already measured quite well, the degradation is not as harmful.

Adding higher harmonics to the signal substantially improves these results. In some cases, measurement errors for aligned systems can be brought below the error level for random spin orientations without higher harmonics. For the mass measurements, this improvement happens in every case. The minor axis of the sky position error ellipse and luminosity distance achieve this benchmark less often, though still in the majority of cases, while the major axis and the spin magnitudes do not fare as well. Sometimes parameters are actually determined a bit better for aligned spins than for random ones thanks to the increased SNR measured for aligned spin systems. For mass measurements, this happens in almost every case we considered.

Although studies like [16] and this one are starting to finalize expectations for LISA's parameter estimation capabilities, several avenues of research into the problem still remain. First is the issue of including proper astrophysical information, such as the possibility of partially aligned spins, when analyzing LISA science. Another example is the recent realization that eccentricity may need to be included in the waveform model (with a first analysis by Key and Cornish [18]). In order to make reliable estimates of LISA's science capabilities, future studies must continue to incorporate the newest astrophysical developments. It will also be useful to turn the problem around and ask what LISA measurements of properties like spin alignment can tell us about the surrounding gas (or lack thereof). It may be possible, from the gravitational waves alone, to predict the nature of an electromagnetic counterpart or to make statements about a binary's environment in case a counterpart is missed. We plan to study this issue in more detail in the future.

Lacking from our Fisher-matrix-based study is an investigation of how the spin-alignment priors of the hot, cold, and dry scenarios may affect parameter estimation. In a more thorough Bayesian analysis, the range of spin alignments for each model can be included as priors. Bayesian model selection can then be used to identify the model that best describes the data. For cold gas mergers, the tight priors on the spin-orbit alignment would translate into improvements in the parameter estimation over what we have found here. Thus, the spin-alignment priors can help put back some of parameter recovery accuracy that is taken away by the suppression of the spin precession. We are currently investigating this issue.

An obvious avenue for LISA parameter estimation studies is the improvement of the waveform model. While the inspiral is nearly complete, the study of the merger is just beginning. In the next few years, complete inspiral waveforms from codes like this one will be joined to effective-one-body waveforms for the late inspiral, fits to numerical models of the merger, and perturbative ringdowns to give a complete LISA waveform for analysis purposes. While such studies have begun [17,19], they do not yet include spins. Including the merger and ringdown is critical; not

only do they provide a great deal of SNR and parameter information, but they also provide a physical tapering of the waveform. The results of this paper unfortunately do not always quantitatively match those of Paper I and [16] when appropriate, primarily because the earlier studies use the stationary phase approximation while we taper the signal and apply an FFT. In essence, despite the use of the MECO, we are applying an earlier cutoff and losing some information about our parameters. When the complete signal is used, choices of cutoff will become irrelevant, and different results should agree more readily. Of course, for this paper, exact error estimates are not the end goal; instead, we have aimed only to show general behavior and trends which are independent of any shift in the baseline error values.

Finally, the Fisher-matrix formalism itself must be checked to make sure it is correct with complicated waveforms and large numbers of parameters. We plan to carry out a comparison between this code's results and those obtained by exploring the full posterior probability using Markov Chain Monte Carlo techniques [48–51]. Early results have shown that the Fisher matrix is indeed still valid in most regimes—a relief given that Markov Chain Monte Carlo techniques cannot as easily survey a plethora of sky locations and orientations—but the full parameter space has not been explored. It is clear, however, that care must be taken with all three areas, astrophysics, general relativity, and statistical analysis, before a final picture of LISA science capabilities can be established.

ACKNOWLEDGMENTS

We thank Cole Miller for suggesting the problem to us. We also thank Samaya Nissanke, Sean McWilliams, and Tyson Littenberg for useful discussions. R. N. L. was supported by an appointment to the NASA Postdoctoral Program at the Goddard Space Flight Center, administered by Oak Ridge Associated Universities through a contract with NASA. This work is supported at MIT by NASA Grant NNX08AL42G and NSF Grant PHY–0449884. S. A. H. in addition gratefully acknowledges the support of the Adam J. Burgasser Chair in Astrophysics in completing this analysis. N. J. C. was supported by NASA Grant NNX10AH15G.

[1] J. G. Baker, S. T. McWilliams, J. R. van Meter, J. Centrella, D.-I. Choi, B. J. Kelly, and M. Koppitz, Phys. Rev. D **75**, 124024 (2007).
[2] A. Sesana, M. Volonteri, and F. Haardt, Mon. Not. R. Astron. Soc. **377**, 1711 (2007).
[3] C. Cutler, Phys. Rev. D **57**, 7089 (1998).
[4] S. A. Hughes, Mon. Not. R. Astron. Soc. **331**, 805 (2002).
[5] A. Vecchio, Phys. Rev. D **70**, 042001 (2004).
[6] E. Berti, A. Buonanno, and C. M. Will, Phys. Rev. D **71**, 084025 (2005).
[7] D. E. Holz and S. A. Hughes, Astrophys. J. **629**, 15 (2005).
[8] E. Berti, V. Cardoso, and C. M. Will, Phys. Rev. D **73**, 064030 (2006).
[9] R. N. Lang and S. A. Hughes, Phys. Rev. D **74**, 122001 (2006); and , **75**, 089902(E) (2007); and , **77**, 109901(E) (2008).
[10] K. G. Arun, B. R. Iyer, B. S. Sathyaprakash, and S. Sinha, Phys. Rev. D **75**, 124002 (2007).
[11] K. G. Arun, B. R. Iyer, B. S. Sathyaprakash, S. Sinha, and C. van den Broeck, Phys. Rev. D **76**, 104016 (2007).
[12] M. Trias and A. M. Sintes, Phys. Rev. D **77**, 024030 (2008).
[13] R. N. Lang and S. A. Hughes, Astrophys. J. **677**, 1184 (2008).
[14] E. K. Porter and N. J. Cornish, Phys. Rev. D **78**, 064005 (2008).
[15] R. N. Lang and S. A. Hughes, Classical Quantum Gravity **26**, 094035 (2009).
[16] A. Klein, P. Jetzer, and M. Sereno, Phys. Rev. D **80**, 064027 (2009).
[17] S. T. McWilliams, J. I. Thorpe, J. G. Baker, and B. J. Kelly, Phys. Rev. D **81**, 064014 (2010).
[18] J. S. Key and N. J. Cornish, Phys. Rev. D **83**, 083001 (2011).
[19] S. T. McWilliams, R. N. Lang, J. G. Baker, and J. I. Thorpe, arXiv:1104.5650.
[20] L. S. Finn, Phys. Rev. D **46**, 5236 (1992).
[21] C. Cutler and É. É. Flanagan, Phys. Rev. D **49**, 2658 (1994).
[22] K. A. Arnaud, S. Babak, J. G. Baker, M. J. Benacquista, N. J. Cornish, C. Cutler, S. L. Larson, B. S. Sathyaprakash, M. Vallisneri, A. Vecchio *et al.*, in *Laser Interferometer Space Antenna: 6th International LISA Symposium*, American Institute of Physics Conference Series Vol. 873, edited by S. M. Merkowitz and J. C. Livas (2006), pp. 619–624.
[23] P. J. Armitage and P. Natarajan, Astrophys. J. Lett. **567**, L9 (2002).
[24] J. N. Bode and E. Phinney, Bull. Am. Astron. Soc., **41**, 341 (2009).
[25] S. M. O'Neill, M. C. Miller, T. Bogdanović, C. S. Reynolds, and J. D. Schnittman, Astrophys. J. **700**, 859 (2009).
[26] M. Milosavljević and E. S. Phinney, Astrophys. J. Lett. **622**, L93 (2005).
[27] N. Stone and A. Loeb, Mon. Not. R. Astron. Soc. **412**, 75 (2011).
[28] C. Wegg and J. N. Bode, arXiv:1011.5874.
[29] J. A. Tyson, in *Survey and Other Telescope Technologies and Discoveries* , edited by J. A. Tyson and S. Wolff, SPIE

Conference Series, Vol. 4836 (SPIE, Bellingham, WA, 2002), pp. 10–20.
[30] T. A. Apostolatos, C. Cutler, G. J. Sussman, and K. S. Thorne, Phys. Rev. D **49**, 6274 (1994).
[31] L. E. Kidder, Phys. Rev. D **52**, 821 (1995).
[32] T. Bogdanović, C. S. Reynolds, and M. C. Miller, Astrophys. J. Lett. **661**, L147 (2007).
[33] M. Dotti, M. Volonteri, A. Perego, M. Colpi, M. Ruszkowski, and F. Haardt, Mon. Not. R. Astron. Soc. **402**, 682 (2010).
[34] K. G. Arun, S. Babak, E. Berti, N. Cornish, C. Cutler, J. Gair, S. A. Hughes, B. R. Iyer, R. N. Lang, I. Mandel *et al.*, Classical Quantum Gravity **26**, 094027 (2009).
[35] P. C. Peters, Phys. Rev. **136**, B1224 (1964).
[36] P. J. Armitage and P. Natarajan, Astrophys. J. **634**, 921 (2005).
[37] J. Cuadra, P. J. Armitage, R. D. Alexander, and M. C. Begelman, Mon. Not. R. Astron. Soc. **393**, 1423 (2009).
[38] A. Sesana, Astrophys. J. **719**, 851 (2010).
[39] A. Buonanno, Y. Chen, and M. Vallisneri, Phys. Rev. D **67**, 104025 (2003).
[40] M. Boyle, D. A. Brown, L. E. Kidder, A. H. Mroué, H. P. Pfeiffer, M. A. Scheel, G. B. Cook, and S. A. Teukolsky, Phys. Rev. D **76**, 124038 (2007).
[41] S. G. O'Sullivan and S. A. Hughes, Phys. Rev. D (to be published).
[42] L. J. Rubbo, N. J. Cornish, and O. Poujade, Phys. Rev. D **69**, 082003 (2004).
[43] M. Vallisneri, Phys. Rev. D **71**, 022001 (2005).
[44] A. Petiteau, G. Auger, H. Halloin, O. Jeannin, E. Plagnol, S. Pireaux, T. Regimbau, and J. Vinet, Phys. Rev. D **77**, 023002 (2008).
[45] J. W. Armstrong, F. B. Estabrook, and M. Tinto, Astrophys. J. **527**, 814 (1999).
[46] J. Crowder and N. J. Cornish, Phys. Rev. D **75**, 043008 (2007).
[47] L. Blanchet, Living Rev. Relativity **9**, 4 (2006), http://relativity.livingreviews.org/Articles/lrr-2006-4/.
[48] N. Christensen and R. Meyer, Phys. Rev. D **64**, 022001 (2001).
[49] N. J. Cornish and J. Crowder, Phys. Rev. D **72**, 043005 (2005).
[50] N. J. Cornish and E. K. Porter, Classical Quantum Gravity **23**, S761 (2006).
[51] N. J. Cornish and E. K. Porter, Phys. Rev. D **75**, 021301 (2007).